Microstructures of $La_{1-x}A_x$(A = Ca or Sr)$MnO_{3-\delta}$ thin films by liquid-delivery metalorganic chemical vapor deposition

Y. Xin and K. Han
Magnet Science and Technology, National High Magnetic Field Laboratory, Florida State University, Tallahassee, Florida 32310

N. Mateeva
Department of Chemistry and MARTECH, Florida State University, Tallahassee, Florida 32306

H. Garmestani
Department of Mechanical Engineering, FAMU-FSU College of Engineering, Tallahassee, Florida 32306

P.N. Kalu
Magnet Science and Technology, National High Magnetic Field Laboratory, Florida State University, Tallahassee, Florida 32310, and Department of Mechanical Engineering, FAMU-FSU College of Engineering, Tallahassee, Florida 32306

K-H. Dahmen
Department of Chemistry and MARTECH, Florida State University, Tallahassee, Florida 32306

(Received 4 January 2001; accepted 8 August 2001)

The microstructure of $La_{1-x}A_x$(A = Ca or Sr)$MnO_{3-\delta}$ thin films grown by liquid-delivery metalorganic chemical vapor deposition on (001) MgO and $(110)_{pseudo\text{-}cubic}$ $LaAlO_3$ were studied by transmission electron microscopy. The $La_{1-x}Ca_xMnO_{3-\delta}$ thin film on large lattice mismatched MgO exhibited very defective microstructures and consisted of two typical regions. The first region was close to the film–substrate interface and had an epitaxial relationship to the substrate with many differently oriented domains nucleated on the substrate surface. The second region consisted of columnar grains with some degree of texture. In contrast, the smaller lattice-mismatched $La_{1-x}Sr_xMnO_{3-\delta}/(110)_{pseudo\text{-}cubic}$ $LaAlO_3$ film had good crystalline quality with highly oriented columnar grains but exhibited complicated dislocation structures. Apart from the misfit dislocations formed at the film–substrate interface, two types of anomalous dislocations with limited contribution to relieving misfit stresses were also observed. One type of dislocation had extra planes in the film and some climbed into the substrate. These dislocations were considered to form from dislocation loops during nucleation of the film. The other type of dislocations had extra planes parallel to the film–substrate interface and glided into the substrate side resulting in a 2° tilt of the film with respect to the substrate. The complicated dislocation configurations present in the sample were related to the complex strain field in the film. The relative strains along the interface measured in the film were heterogeneous. The variations of the strains in the film were related to the local Curie temperature changes and second-order phase transitions of the film.

I. INTRODUCTION

Perovskite manganites $R_{1-x}A_xMnO_3$, where R denotes trivalent rare-earth elements, and A divalent alkaline-earth elements, have attracted much attention recently due to their interesting electronic and magnetic properties, including colossal magnetoresistance (CMR) phenomena,[1] making them attractive candidates for potential device applications. Various methods have been used to fabricate $R_{1-x}A_xMnO_3$ materials with a wide range of compositions and crystal structures. Particular attention has been paid to the fabrication of $La_{1-x}A_x$(A = Ca or Sr)$MnO_{3-\delta}$ thin films because of their promising potential for devices.

The most common deposition method used for the growth of manganite thin films is pulsed laser deposition, although magnetron sputtering,[2,3] metalorganic chemical vapor deposition (MOCVD),[4–7] and dipping-pyrolysis[8] are also employed. The substrates used are usually $SrTiO_3$, $LaAlO_3$, MgO, Y-stabilized ZrO_2, and Al_2O_3 with lattice mismatch ranging from less than 1% to 9%.

It was well documented that the microstructure and the strain or even the film thickness had strong influences on their physical properties, such as the change of resistivity, magnetoresistivity, and Curie temperatures.[7,9–18] The lattice mismatch between the thin film and the substrate is a consequential parameter having a great influence on the structure, morphology, and strain of the thin films. The films grown on a large lattice mismatched substrate, such as MgO with a mismatch of 8% usually have relaxed lattice parameters which are close to the bulk material.[13,19] However, on small lattice mismatched substates, such as $SrTiO_3$ or $LaAlO_3$, the films usually have lattice distortions, and the resulting strain of the film depends largely on the film thickness and annealing conditions.[14,20,21]

Currently, defects in perovskite oxide thin films are poorly characterized in comparison to semiconductor materials, even though the structural defects have a strong influence on the properties of the CMR materials. Therefore, it is necessary to examine the detailed microstructure of the thin films, particularly in light of the strong interplay between electrons and crystal lattice. It is noted that the main microstructural features for the $La_{1-x}Ca_xMnO_{3-\delta}$ (LCMO) films are the domains formed with different crystallographic orientations.[19,20,21] The films deposited on $SrTiO_3$, which has the smallest lattice mismatch, were observed to consist of domains. Defects, such as twin domains and antiphase boundaries have been observed. On the other hand, $La_{1-x}Sr_xMnO_{3-\delta}$ (LSMO) films usually grow into single domain with fewer defects, while the strain is dependent on the film thickness.

To illustrate the microstructure of both LCMO and LSMO thin films, two extreme cases were selected, i.e., LCMO on large mismatched MgO, and LSMO on small mismatched $LaAlO_3$. Hence, this paper concentrates on the microstructural characterization of the $La_{1-x}Ca_xMnO_{3-\delta}$ thin film grown on (001) MgO and $La_{1-x}Sr_xMnO_{3-\delta}$ on $(110)_{pseudo\text{-}cubic}$ $LaAlO_3$ substrates by liquid-delivery MOCVD. Various transmission electron microscopy (TEM) techniques were utilized to illustrate the microstructure and atomic structure of the films. The growth mechanism and the effect of defects on the physical properties are tentatively discussed.

II. EXPERIMENTAL DETAILS

$La_{1-x}A_x$(A = Ca or Sr)$MnO_{3-\delta}$ (with nominal x about 0.3) thin films were grown on (001)MgO and $(110)_{pseudo\text{-}cubic}$ $LaAlO_3$ substrates by liquid-delivery MOCVD. The precursors $La(tmhd)_3$, $Mn(tmhd)_3$, $Sr(tmhd)_3$, and $Ca(tmhd)_3$, were mixed and diluted with a standard solvent, and then were continuously injected into an EMCORE commercial reactor, modified with a NZ-Applied Technologies liquid delivery system. The vaporized precursors were transported to the deposition chamber by N_2 and O_2 gas carriers. The substrate temperature was held at 600 to 700 °C during the growth process. After deposition, the films were slowly cooled down to below 100 °C before removal. More detailed information on the growth conditions and deposition process can be found in Refs. 5 and 16.

An *ex-situ* TEM analysis was performed using a Jeol-2010 analytical electron microscope operated at 200 kV with a point resolution of 0.23 nm and lattice resolution of 0.14 nm. Cross-sectional TEM samples were prepared by conventional methods.

III. RESULTS

A. $La_{1-x}Ca_xMnO_{3-\delta}$/(001)MgO thin film

The crystal structure of $La_{1-x}A_xMnO_{3-\delta}$ could be described as an orthorhombic unit cell that is closely related to the perovskite structure. The relation between the lattice parameters of the two types of unit cells can be written as $a_o \approx \sqrt{2}\, a_p$, $b_o \approx 2a_p$, and $c_o \approx \sqrt{2}\, a_p$, where a_o, b_o, c_o, and a_p correspond to the lattice parameters of the orthorhombic and perovskite unit cell, respectively. The indexing used in the current paper is based on the orthorhombic unit cell.

The LCMO thin film on (001) MgO substrate has three different regions related to different growth mechanisms, as shown in Figs. 1(a) and 1(b). Region I is about 20 nm in thickness located just below the film–substrate interface in the MgO substrate. It shows a different contrast from the MgO substate. Region II is an epitaxial LCMO region of about 100 nm in thickness, which lies above the film–substrate interface. Region III extends up to the film surface and contains a polycrystalline structure [Figs. 1(a) and 1(b)]. Intermixing of elements was found by energy dispersive x-ray spectroscopy (EDS) analysis using a 5-nm probe positioned at various discrete points in both the substrate and the film, as shown in Fig. 2. In the following text, different regions are discussed in detail.

Manganese was found in the pits of region I below the film–substrate interface. Manganese has solubility in magnesium oxide by replacing magnesium atoms to form various manganese magnesium oxides. Therefore, region I is a product of the early stage of deposition in which reaction occurs. Detailed examinations of the high-resolution TEM (HRTEM) image showed the lattice parameters of the (Mg, Mn)O in region I equal to that of pure MgO. In both regions II and III, LCMO crystals formed, but they had different morphologies [Fig. 1(a)]. Region II is in the vicinity of the substrate surface and shows a streaky contrast in the low magnification image. Selected-area diffraction patterns show that LCMO formed in this region has an epitaxial crystal growth

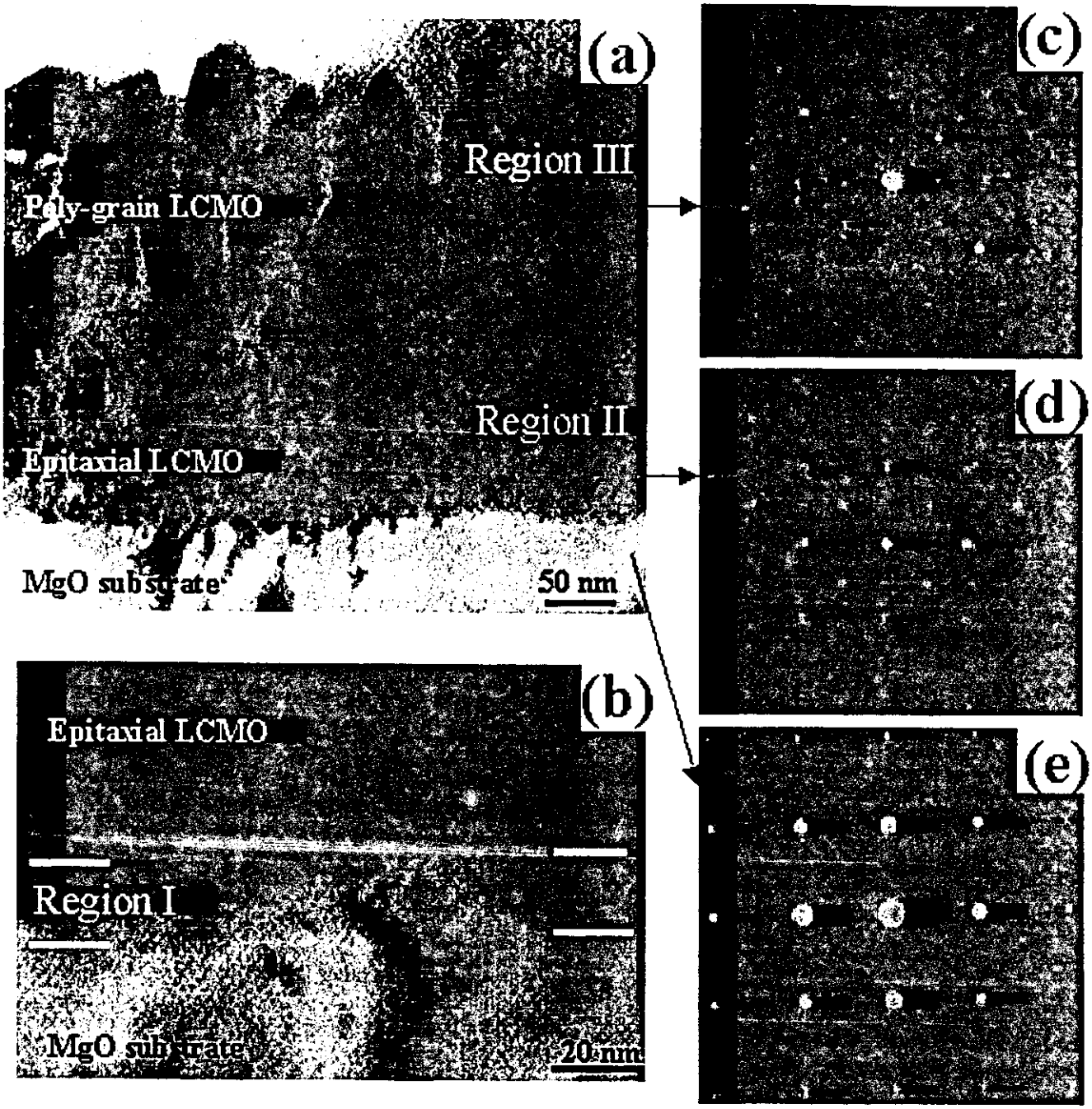

FIG. 1. TEM cross-sectional images and SADP from LCMO thin film on (001) MgO substrate showing various regions formed during the growth: (a) low-magnification, bright-field (BF) TEM image; (b) BF image of the interface reigon showing the pitlike contrast in MgO substrate delineating the interface; (c) SADP from the polycrystalline region; (d) SADP from the interface region; and (e) SADP from MgO substrate.

relationship with MgO substrate [Fig. 1(d)]. EDS analysis showed that this region was La deficient and some magnesium was detected.

The calculated misfit $f = (a_{\text{substrate}} - a_{\text{epilayer}})/a_{\text{substrate}}$ for LCMO/MgO is 8.7%, with the epilayer under tensile stresses. The misfit measured from the selected-area diffraction pattern (SADP) [Fig. 1(d)] is about 8%, indicating that the mismatch strain is mostly relieved by forming misfit dislocations. The measurement of the lattice planes across the relatively flat interface region gives an extra plane in LCMO about every 12 planes, corresponding to an average misfit dislocations distance of 5 nm with Burgers vector $\mathbf{b} = \mathbf{a}_p$. Such a misfit dislocation configuration relieves the mismatch completely, and this is consistent with the SADP results.

Figure 3 is a HRTEM image showing the detailed atomic arrangement at the interface region and the fast Fourier transform (FFT) patterns from different

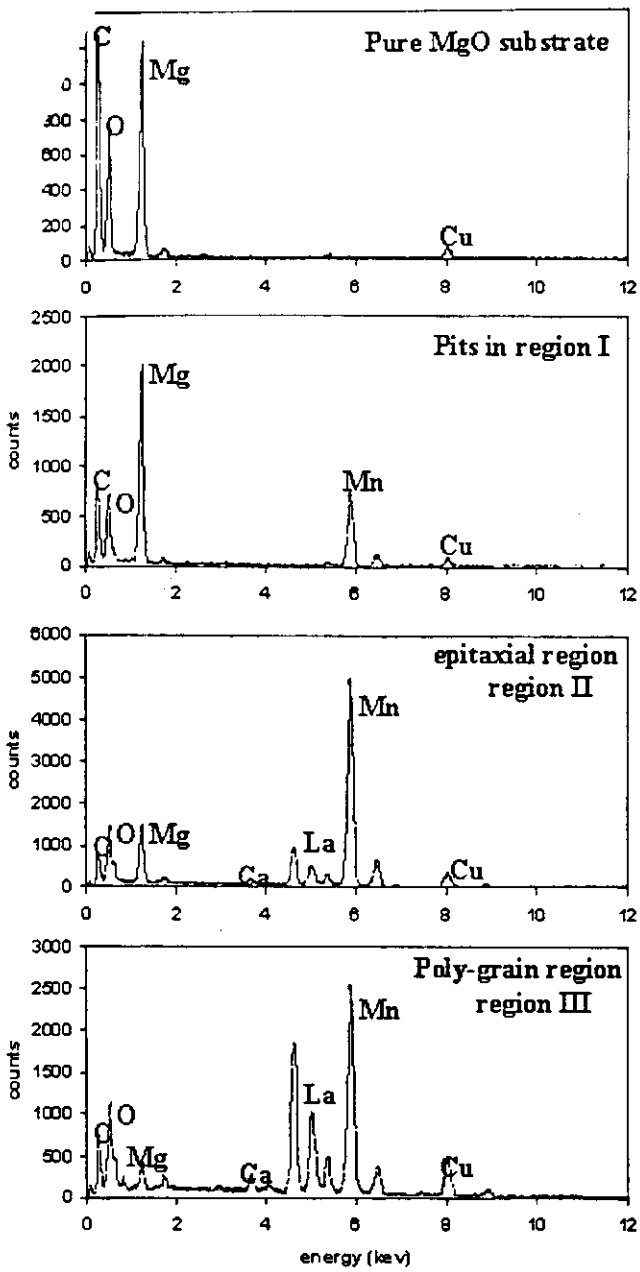

FIG. 2. EDS spectra from the different regions showing the diffusion of Mn into the MgO substrate, which formed the pits.

areas. The interface between the film and the substrate is not flat on the nanometer scale. The MgO substrate surface forms steps. The step height along $[001]_{MgO}$ is between 1 and 5 nm. Within the LCMO film of region II, domains with three different orientations with respect to the [001]MgO were found in addition to planar defects. The domains apparently were formed by homogeneous nucleation and island growth of LCMO. The nominal size of the domains is about 30 nm. The orientations between the LCMO domains and MgO are (i) $[101]_{LCMO}//[100]_{MgO}$ with $(020)_{LCMO}//(002)_{MgO}$, (ii) $[010]_{LCMO}//[100]_{MgO}$ $(020)_{LCMO} \perp (002)_{MgO}$, and (iii) $[101]_{LCMO}//[010]_{MgO}(020)_{LCMO}//(020)_{MgO}$, where $(002)_{MgO}$ is the atomic plane parallel to the nominal MgO surface and $(020)_{MgO}$ is the atomic plane perpendicular to the MgO surface. The atomic planes parallel to the nominal LCMO/MgO interfaces in different domains are not parallel to each other, and some are displaced up to half of the lattice spacing in the growth direction. In some domains, the FFT reveals the (010) forbidden reflections that result from either symmetry change,[21] or crystal tilt.[22]

In region III, columnar growth occurs. The columns have various orientations and show almost no epitaxial relationship with the substrate.

B. $La_{1-x}Sr_xMnO_{3-\delta}/(110)_{pseudo\text{-}cubic}$ $LaAlO_3$ thin film

The LSMO[23] film grown on the smaller lattice mismatched $LaAlO_3$ $(110)_{pseudo\text{-}cubic}$ substrate exhibits much better crystallinity, and a strikingly different microstructure from LCMO grown on the MgO substrate if one compares Figs. 1 and 4.

$LaAlO_3$ has a rhombohedrally distorted perovskite structure at room temperature,[24] with space group $R\bar{3}c$, and becomes a cubic perovskite above 435 °C.[25] A hexagonal unit cell with $a = 5.3655$, $c = 13.112$ could be used to index the diffraction pattern properly. The SADP from the $LaAlO_3$ substrate of the cross-sectional sample [Fig. 4(d)] is along the $[\bar{1}101]$ zone axis of the hexagonal unit cell, which is $[\bar{1}10]$ using a pseudo-cubic unit cell. For simplicity and convenience, a pseudo-cubic cell of $LaAlO_3$ is used to describe the crystallographic geometry and dislocation features in the following discussion.

The thin film is about 367 nm thick and exhibits a single-crystal pattern, as shown by a [100] SADP in Fig. 4(c). The film is composed of highly oriented columnar grains about 60 nm in width with narrow gaps between grains [Fig. 4(b)]. The orientation relationship between LSMO film and the substrate is $[001]_{LSMO}//[1\bar{1}0]_{LaAlO_3}$, $[100]_{LSMO}//[1\bar{1}0]_{LaAlO_3}$, $[010]_{LSMO}//[001]_{LaAlO_3}$. Many dislocations were observed near the film–substrate interface in the $LaAlO_3$ substrate [Fig. 4(a)]. The lattice parameter measurement by SADP [Figs. 4(e) and 4(f)] shows a mismatch of 3.1% along the $[001]_{LaAlO_3}$ in-plane direction. If the pseudo-cubic lattice parameter of $LaAlO_3$ is taken as 0.379 nm[25] the in-plane lattice parameter of LSMO is calculated to be about 0.391 nm.

Figure 5 is a HRTEM image showing the atomic arrangement in the vicinity of the film–substrate interface. The interface is relatively flat with a modulation of only a few atomic monolayers. The LSMO film grows epitaxially on the substrate surface, and Moiré fringes are observed. The Moiré fringes are related to overlapping of the grains with slightly different orientation formed during nucleation and growth.

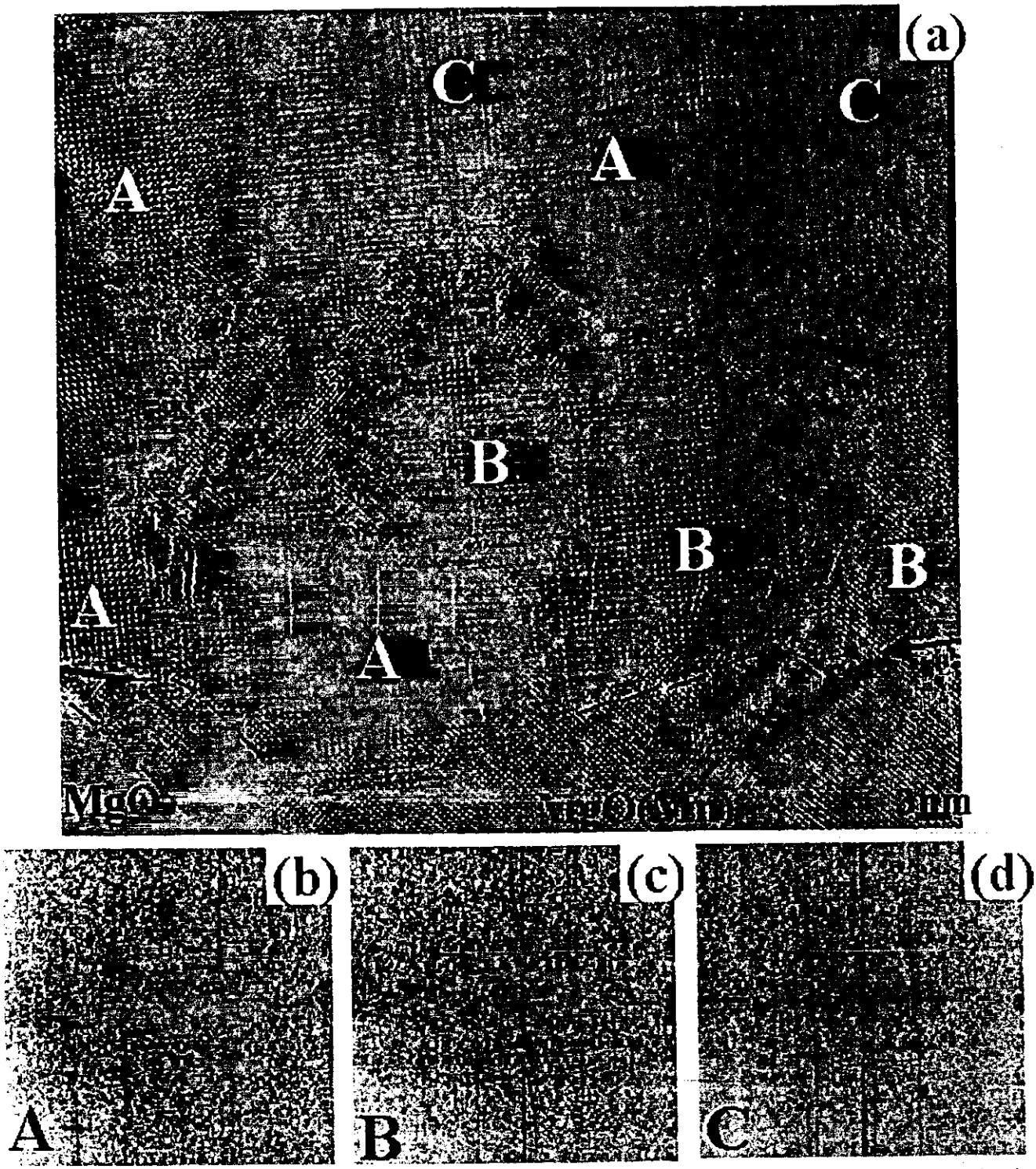

FIG. 3. HRTEM image and the FFT diffraction patterns from different orientated domains showing the detailed atomic structures of the interface regions. The interface between LCMO and (MgMn)O is indicated by arrows and thick dotted lines. The interfaces between MgO and Mg,MnO is indicated by thin dotted lines. (a) HRTEM image. (b) FFT from domain A down [101] zone axis. (c) FFT from domain B down [010] zone axis. (d) FFT from domain C with [101] zone axis but the pattern rotated 90° with respect to domain A.

Dislocations present in this sample could be divided into two categories: those at the interface, and those in the $LaAlO_3$ substrate. The dislocations at the interface are shown in Fig. 6. In a conventional TEM bright-field (BF) image [Fig. 6(a)], the sample is tilted along $[001]_{LaAlO_3}$, so that the dislocation arrays at the interface can be examined. The dark lines with oscillating contrast are dislocations, which have an average spacing of about

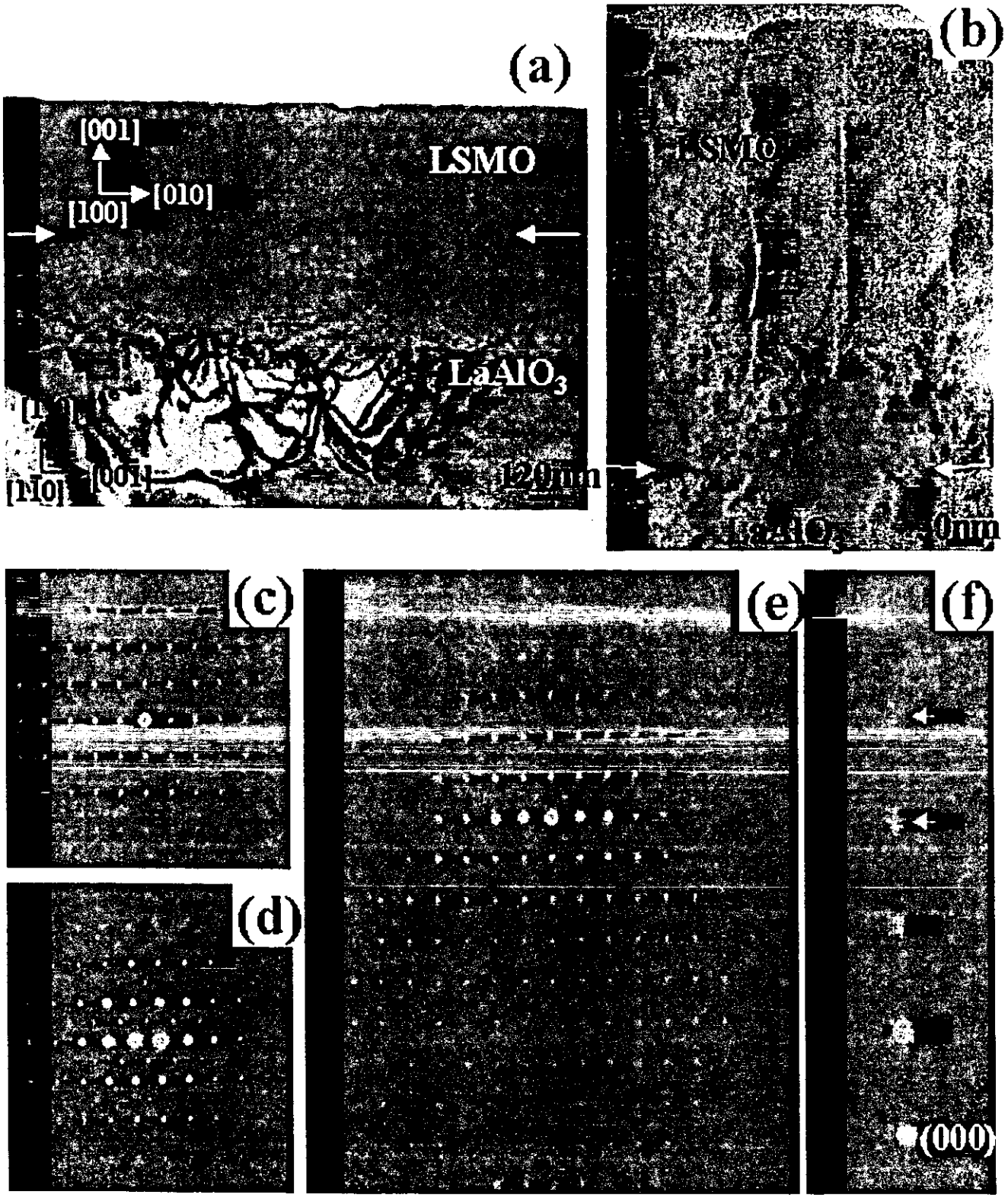

FIG. 4. TEM cross-sectional images and SADP from LSMO/(110)$LaAlO_3$ showing the morphology of the film and dislocation structures in the substrate (The film–substrate interface is indicated by white arrows): (a) BF images showing the dislocation configurations in the substrate; (b) BF images showing the columnar grains in the film; (c) [100] SADP from the LSMO film; (d) $[1\bar{1}0]_{pseudo\text{-}cubic}$ SADP from the $LaAlO_3$ substrate; (e) SADP from the LSMO/$LaAlO_3$ interface; and (f) Enlargement of (020) row diffraction to show the splitting spots from LSMO and $LaAlO_3$, as indicated by arrows.

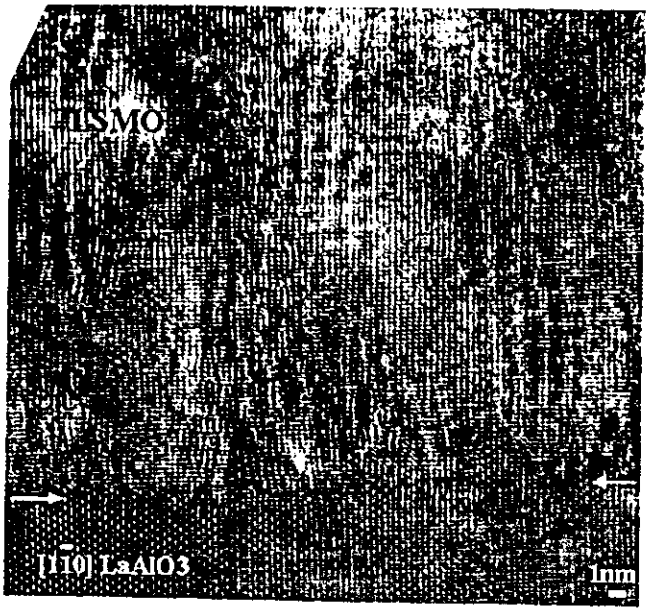

FIG. 5. HRTEM image showing the film–substrate interface region. There are chimney like Moire fringes from the interface.

4.9 nm. It is also noted that some dislocations are extended into the substrate, as indicated by the large arrow. The HRTEM image in Fig. 6(b) demonstrates the detailed atomic configurations of the dislocations. Misfit dislocations are those at the interface that are capable of relieving the mismatch. Because the substrate has smaller lattice spacing than the film, the dislocations that have extra planes in the substrate are misfit dislocations. By drawing a Burgers circuit around such dislocations, as shown in Fig. 6(b), the Burgers vector **b** can be deduced to be $[00\bar{1}]a_{LaAlO_3}$. In addition to misfit dislocations, anomalous dislocations were observed to have an extra plane in the film side, as shown in Fig. 6(b), by the dark line. The average spacing between misfit dislocations is obtained by counting the number of corresponding planes perpendicular to the interface for both the film and the substrate, i.e., $(020)_{LSMO}$ and $(001)_{LaAlO_3}$. There is one extra plane in the substrate for every 24 to 26 (001) $LaAlO_3$ planes, which corresponds to an average spacing of 9.8 nm for the misfit dislocations at the interface. Using the experimental value of the misfit (f) of 3.1%, the calculated dislocation spacing necessary to relieve the mismatch is $d = \mathbf{b}/f = 12.2$ nm. This is consistent with the observed misfit dislocation distribution in the sample within the experimental errors, indicating the mismatch strain is mostly relieved. The dislocations observed in BF images [Fig. 6(a)] include both the misfit dislocations and dislocations with other characters formed in the vicinity of the interface. The average spacing of 4.9 nm observed from bright-field imaging is therefore about half of the misfit dislocation spacing obtained by HRTEM. A combination of the BF and HRTEM results hence indicate that fifty percent of the interfacial

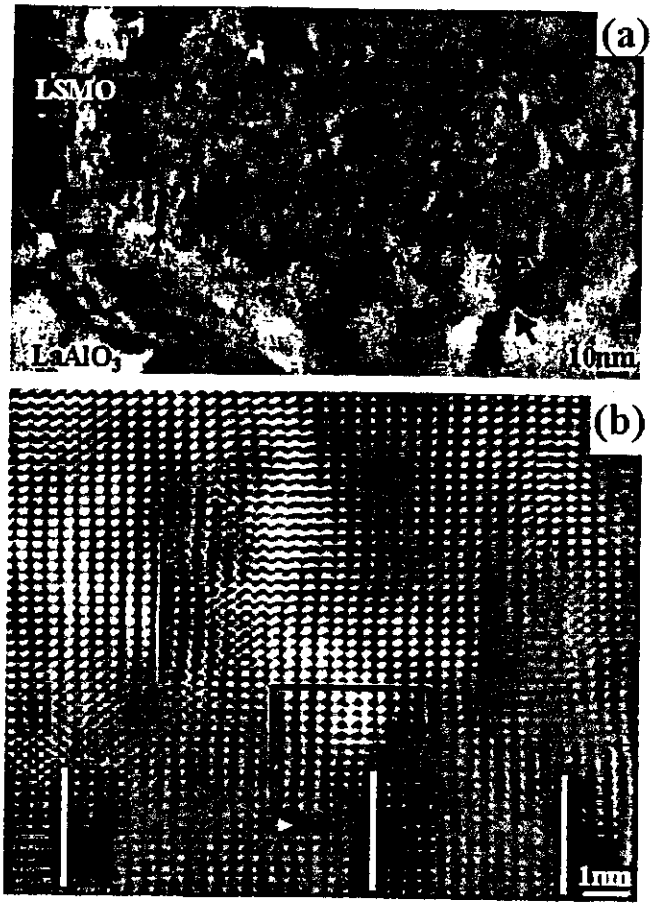

FIG. 6. BF and filtered HRTEM images of LSMO/(110)$LaAlO_3$ interfaces showing the dislocation arrays at the interface: (a) BF image of a tilted film/substrate interface. Some dislocation arrays at the interface are marked by small black arrows. (b) A filtered HRTEM image of the interface region showing misfit dislocation (indicated by white line), and dislocation with the extra plane in the film side (indicated by black line). On misfit dislocation is drawn with a Burgers circuit.

dislocations are the anomalous dislocations that have no direct impact on the mismatch between the substrate and the film.

This intricate dislocation configuration in the interface region indicates a heterogeneous distribution of strains along the interface, as evidenced by the variation of relative strains along the interface. The strain variations ($\Delta\epsilon$) in various regions of the film close to the film–substrate interface were measured by FFT diffraction spots from HRTEM images. $\Delta\epsilon$ is calculated by $(d - d_{aver})/d_{aver}$, where d is the measured lattice spacing and d_{aver} is the average value of the lattice spacing. The plot of the relative strain versus the position along the interface is shown in Fig. 7. The differences of the strains in various areas are manifested in the sketch.

The dislocations present in the $LaAlO_3$ substrate were studied further by weak-beam dark-field TEM. Figure 8 shows a typical cross sectional-sample imaged by **g/3g** with **g** = (110) [Fig. 8(a)] and **g/3g** with **g** = (001)

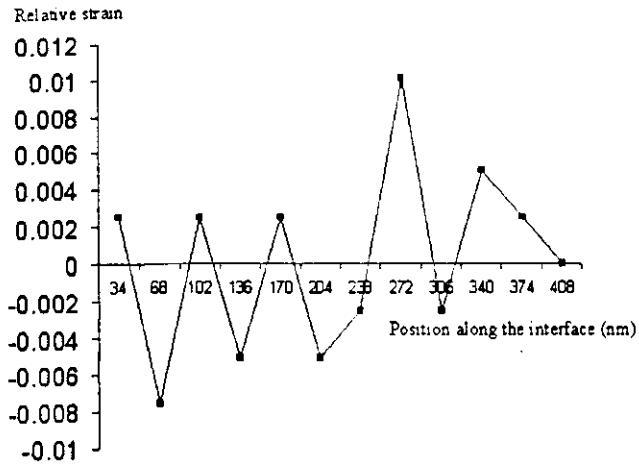

FIG. 7. Plot of relative strain $\Delta\epsilon$ versus positions along the film–substrate interface showing the variation of strains of the film close to the interface. $\Delta\epsilon$ was measured in an area of 35 nm in width.

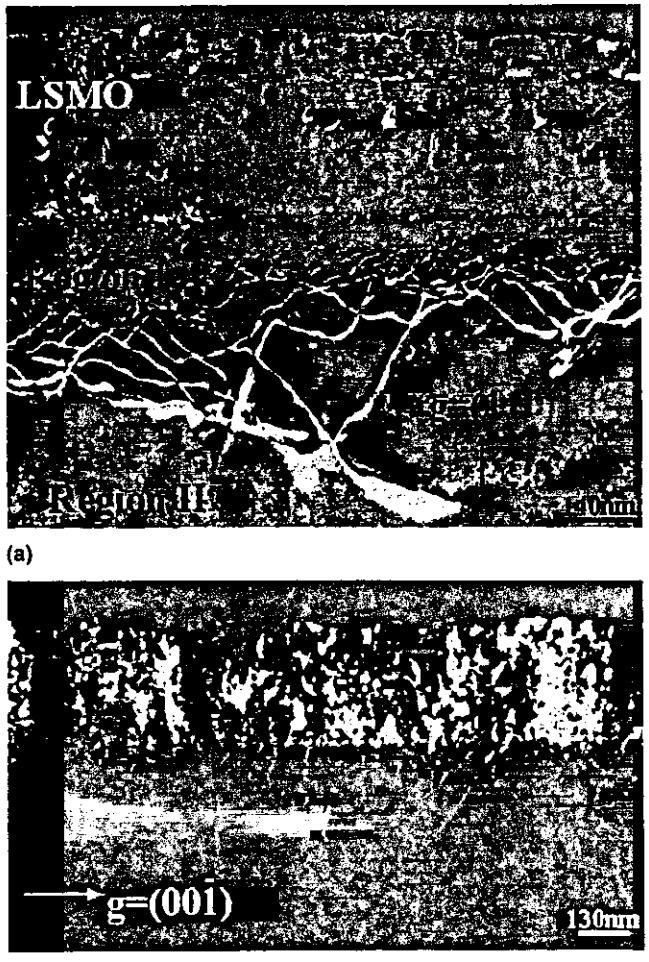

FIG. 8. Weak-beam, dark-field TEM images showing the dislocations in $LaAlO_3$ substrate from LSMO/(110)$LaAlO_3$: (a) **g/3g** weak beam image using **g** = (110); and (b) g/3g weak beam image of the same region as in (a) using **g** = (00$\bar{1}$). The bright dots in the substrates are due to beam damage.

[Fig. 8(b)]. The dislocations are very densely populated, with the dislocation density decreasing with the distance from the interface into the substrate. They have a half-loop shape and seem to bow into the substrate from the interface. For clarity, the substrate region is divided into two regions, with region I as the dislocation area of about 500 to 600 nm in width, and region II referring to the region further down of dislocation-free substrate area. By tilting the sample along [001] and examining the change of projected width of region I, it is deduced that these dislocations are on (1$\bar{1}$0) plane, which is likely to be the gliding plane.

The Burgers vector **b** = (x,y,z) of the dislocations in region I was determined using a combination of **g.b** = 0 criterion in the diffraction contrast imaging, and the Cherns–Preston rules [**g.b** = $n - 1$, where n is the number of the minimum intensities of Laue zone lines crossed by a dislocation in large-angle convergent beam electron diffraction (CBED)].[26] The dislocations are invisible when imaged by **g** = (00$\bar{1}$) [Fig. 8(b)], and hence, all possible **b** are [x y 0]. The exact values of x and y were determined using Laue zone lines in an over-defocused CBED pattern, as shown in Fig. 9. The lines ($\bar{2}2\bar{4}$) and ($\bar{2}3\bar{3}$) are seen to split into 5 and 6 minimum intensities, respectively. This gives $-2x + 2y = -4$, and $-2x + 3y = -5$. Hence, the **b** of these dislocations is determined to be [1$\bar{1}$0], and they seem to be perfect dislocations with no observed dissociation. The extra planes of these dislocations are parallel to the interface, i.e., on (110), which results in region I and the film being tilted along [001] away from [110] of the substrate normal. The exact orientations from the three different distinct regions (regions I and II in the substrate, and the LSMO film) are determined by Kikuchi patterns, which were obtained by focusing the electron probe on these three different regions. When the dislocation-free substrate region II was oriented to an exact [1$\bar{1}$0] zone axis, the other two regions are shown to be 2° off the zone axis.

The other sets of dislocations in the substrate shown in Fig. 8(b) are believed to have a **b** of [001]. They might be connected with the dislocations with extra planes in the film side and rejected from the interface into the substrate via climbing and gliding.

III. DISCUSSION

It has been well documented that $La_{1-x}A_xMnO_{3-\delta}$ thin films grown on different lattice mismatched substrates exhibit very different morphologies, as was also observed in this study. The growth mechanism is elucidated by the microstructure examinations shown in the last section. When the vapor was deposited on the MgO, a

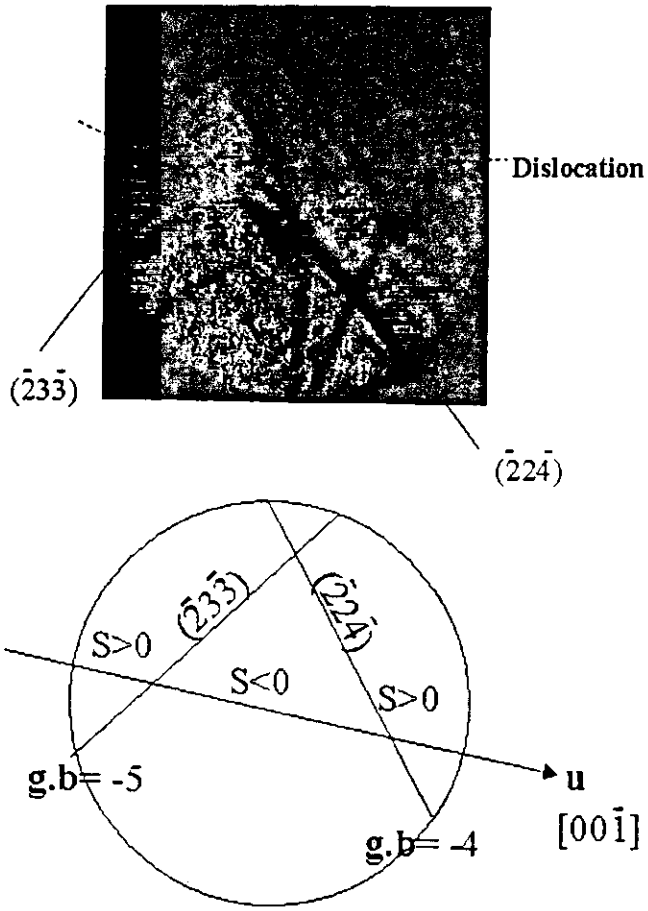

FIG. 9. A defocused CBED pattern with one dislocation from the substrate crossing the Laue zone lines, and its schematic to show the diffraction condition assignment. S is the deviation parameter.

reaction occurred before the nucleation of LCMO, because of the large solubility of Mn in MgO. The interfaces between (Mg,Mn)O and the MgO are faceted on {110} type of planes, indicating that the reaction is interface controlled. Our examination showed that the product of the reaction, (Mg,Mn)O, has similar lattice parameter to that of MgO. Therefore, the reaction introduces no significant change of the misfit between the thin films and the reacted substrate compared with the one between the thin films and virgin substrate. The film with the large lattice mismatch to the substrate resulted in a three dimensional nucleation, with the LCMO nuclei deposited on the surface with orientations of [010] and [101], as they are equivalent variants due to the similar mismatch to the substrate. A shift of the atomic planes in the growth direction suggests that the domains are nucleated independently. Clearly, the nucleation sites on the surface steps with different height result in such a shift. As growth proceeds, this defective layer increases in thickness giving a very irregular and uneven growth front with less restaining effect from the substrate. Therefore, the subsequent growth could easily produce columnar grains with random orientations, as observed. In view of the quality of the film, this LCMO film is not expected to have good physical properties.[9]

Although the LSMO film on (110) $LaAlO_3$ also grew into columns and the film thickness is well beyond the critical thickness for a mismatch of about 3%, it exhibits much better crystalline quality than LCMO on MgO under similar growth conditions. Apparently, the smaller lattice mismatch and the smooth substrate surface assisted the high-quality crystal growth with fewer defects than in LCMO on MgO. The only defects are the various dislocations generated.

The schematic illustrated in Fig. 10 depicts the dislocation configurations in this sample. The (110) substrate orientation determines the geometry of the dislocation network at the interface, with one set of dislocations having a line direction of $[1\bar{1}0]$ and $\mathbf{b} = [00\bar{1}]$ of [001], the other orthogonal set along $[00\bar{1}]$ having $\mathbf{b} = [1\bar{1}0]$ or $[\bar{1}\bar{1}0]$ [Fig. 10(a)]. The dislocations along $[1\bar{1}0]$ consist of anomalous dislocations with $\mathbf{b} = [001]$ and misfit dislocations ($\mathbf{b} = [00\bar{1}]$) that relieve the in-plane mismatch strain, as observed by HRTEM. These dislocations are considered to form from dislocation loops nucleated on the interface plane during initial growth of the LSMO film. As their glide plane is (110), the interface plane, they expand to form the observed dislocations with opposite signs [Fig. 10(b)]. Therefore, these two types of dislocations originate from the same source. The third type of dislocations, which are along $[00\bar{1}]$, are misfit dislocations ($\mathbf{b} = [1\bar{1}0]$) residing at the interface that act to relieve the misfit along $[00\bar{1}]$. The fourth type of dislocations in the substrate with $\mathbf{b} = [\bar{1}\bar{1}0]$ originated from the film–substrate interface during growth. Their glide plane is $(1\bar{1}0)$ which is perpendicular to the film–substrate interface, and their Burgers vectors have extra planes parallel to the interface plane, which do not relieve the mismatch strain directly. In view of the smaller shear modulus of the LSMO film, these dislocations might have been rejected from the interface [Fig. 10(c)] into the substrate due to the misfit stress and the imperfection of the film relative to the substrate during the growth.

It is evident that the mismatch strain in LSMO film is mostly relieved by the midfit dislocations, which are, however, accompanied by additional anomalous dislocations. Such a complex dislocation configuration results in the heterogeneous distribution of the strains in the film, as shown in Fig. 7. It has been found that the Currie temperature T_c and metal–insulator transition temperature is very sensitive to the strains[14,18] due to the Jahn–Teller splitting induced by biaxial strains. The temperature coefficient $\alpha = 1/T_c\, dT_c/d\epsilon$ was estimated to be about 6 for $La_{0.83}Sr_{0.17}MnO_3$.[18] The variation of $\Delta\epsilon$ in different areas was estimated and shown in Fig. 7. The

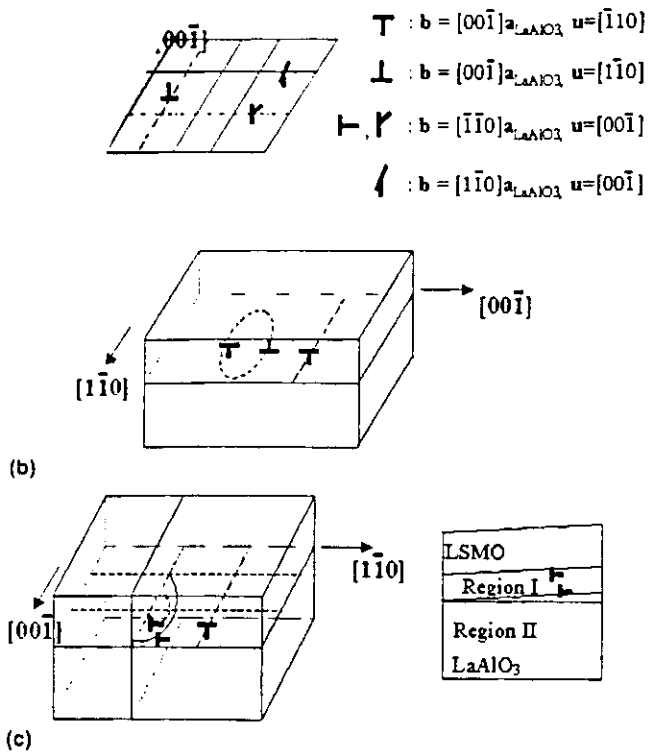

FIG. 10. Schematics showing the dislocation configurations in the LSMO/(110)$LaAlO_3$ thin film: (a) dislocation arrays at the film/substrate interface plane; (b) the view along [1$\bar{1}$0] to show the generation of dislocation loops; and (c) the view along [00$\bar{1}$] showing the dislocations with extra planes parallel to the interface plane pushed into the substrate side, which caused the tilt of region I of the $LaAlO_3$ and LSMO film.

maximum $\Delta\epsilon$ is about 0.01. The dT_c/T_c value is calculated to be about 6%. Thus, a variation of T_c is possible in different regions within a single film. Nevertheless, the measured T_c is an average value. When the CMR material reaches a temperature close to T_c, the second order phase transition occurs only in part of the material. The size of the domains should correspond to the oscillation wavelength of the measured relative strains. Apparently, to reduce the variation of T_c within a single film and increase the performance of the CMR for device application, one expects to have films with lower strain variation $\Delta\epsilon$.

IV. CONCLUSIONS

It was observed that the $La_{1-x}Ca_xMnO_{3-\delta}$/(001)MgO and $La_{1-x}Sr_xMnO_{3-\delta}$/$(110)_{pseudo\text{-}cubic}$ $LaAlO_3$ films, which have different lattice mismatch, show very different microstructures, although the misfit is mostly relieved in both films by misfit dislocations formed at the film–substrate interface. For the LCMO film on MgO with 8% misfit, small domains with variant orientations nucleated on the roughened MgO substrate surface at the initial growth. As the film grew thicker with less restraint from the substrate, it grew into columnar grains of different orientations with some degree of texture. In contrast, LSMO film on $(110)_{pseudo\text{-}cubic}$ $LaAlO_3$ with about 3% misfit shows good crystalline quality. A complicated dislocation configuration was observed in this film. Apart from the misfit dislocations, which effectively relieved the mismatch (dislocations along [1$\bar{1}$0] with **b** = [00$\bar{1}$] and those along [00$\bar{1}$] with **b** = [1$\bar{1}$0]), anomalous dislocations were identified. Some dislocations having the extra planes on the film side may have originated from dislocation loops nucleated at the initial growth stage. Dislocations along [00$\bar{1}$] having extra planes parallel to the interace were generated and pushed into the $LaAlO_3$ substrate at high temperature during film growth. Significant variations of the strains were observed in the film. The effects of the heterogreneou strain distributions on Curie temperature were estimated and rationalized. This study demonstrated the necessity of the investigation of the microstructures associated with the thin films for these CMR materials.

ACKNOWLEDGMENTS

This work was carried out at National High Magnetic Field Laboratory supported by the National Science Foundation under Cooperative Agreement No. DMR 95-27035 and the State of Florida. The microscopy facility was in part funded by National Science Foundation Grant No. DMR-9625692.

REFERENCES

1. K. Chahara, T. Ohno, M. Kasai, and Y. Kozono, Appl. Phys. Lett. **63**, 1990 (1993); S. Jin, T.H. Tiefel, M. Mccormack, R.A. Fastnacht, R. Ramesh, and L.H. Chen, Science **264**, 413 (1994), and references therein.
2. E.S. Vlakhov, R.A. Chakalov, R.I. Chakalova, K.A. Nenkov, K. Dorr, A. Handstein, and K.H. Muller, J. Appl. Phys. **83**, 2152 (1998).
3. K.B. Li, Z.Z. Qi, Z.J. Li, J.S. Zhu, and Y.H. Zhang, Thin Solid Films **304**, 386 (1997).
4. Y.Q. Li, J. Zhang, S. Pombrik, S. Dimascio, W. Stevens, Y.F. Yan, and N.P. Ong, J. Mater. Res. **10**, 2166 (1995).
5. K-H. Dahmen and M.W. Carris, J. Alloys Compd. **251**, 270 (1997).
6. G.J. Snyder, R. Hiskes, S. DiCarolis, M.R. Beasley, and T.H. Geballe, Phys. Rev. B **53**, 14434 (1996).
7. K.A. Thomas, P.S.I.P.N. de Silva, L.F. Cohen, A. Hossain, M. Rajeswari, T. Venkatesan, R. Hiskes, and J.L. MacManus-Driscoll, J. Appl. Phys. **84**, 3939 (1998).
8. T. Manabe, T. Fujimoto, I. Yamaguchi, W. Kondo, I. Kojima, S. Mizuta, and T. Kumagai, Thin Solid Films **323**, 99 (1998).
9. S. Jin, T.H. Tiefel, M. Mccormack, H.M. Obryan, L.H. Chen, R. Ramesh, and D. Schurig, Appl. Phys. Lett. **67**, 557 (1995).
10. N-C. Yeh, C-C. Fu, J.Y.T. Wei, R.P. Vasquez, J. Huynh, S.M. Maurer, G. Beach, and D.A. Beam, J. Appl. Phys. **81**, 5499 (1997).
11. J. Aarts, S. Freisem, R. Hendrikx, and H.W. Zandbergen, Appl. Phys. Lett. **72**, 2975 (1998).

s. Rao, D. Lavric, T.K. Nath, C.B. Eom, L. Wu, and F. Tsui, Appl. Phys. **85,** 4794 (1999).

. Gommert, H. Cerva, J. Wecker, and K. Samwer, J. Appl. Phys. **85,** 5417 (1999).

. F.S. Razavi, G. Gross, H-U. Habermeier, O. Lebedev, S. Amelinckx, G. Van Tendeloo, and A. Vigliante, Appl. Phys. Lett. **76,** 15 (2000).

15. T.K. Nath, R.A. Rao, D. Lavric, C.B. Eom, L. Wu, and F. Tsui, Appl. Phys. Lett. **74,** 1615 (1999).
16. E.S. Gillman, M. Li, and K-H. Dhmen, J. Appl. Phys. **84,** 6217 (1998).
17. H.L. Ju, K.M. Krishnan, and D. Lederman, J. Appl. Phys. **83,** 7073 (1998).
18. A.J. Millis, T. Darling, and A. Migliori, J. Appl. Phys. **83,** 1588 (1998).
19. M. Arita, A. Sasaki, K. Hamada, A. Okada, J. Hayakawa, H. Asano, M. Matsui, and H. Takahashi, J. Electron Microsc. **48,** 381 (1999).
20. H.W. Zandbergen, J. Jansen, S. Freisem, T. Nojima, and J. Aarts, Philos. Mag. A**80,** 337 (2000).
21. G. Van Tendeloo, O.I. Lebedev, and S. Amelinckx, J. Magn. Magn. Mater. **211,** 73 (2000).
22. H.W. Zandbergen and J. Jansen, Ultramicroscopy **80,** 59 (1999).
23. L. Pinsard, J. Rodriguez-Carvajal, and A. Revcolevschi, J. Alloys Compd **262,** 152 (1997).
24. H. Lehnert, H. Boysen, P. Dreier, and Y. Yu, Z. Kristallogr **215,** 145 (2000).
25. S. Geller and V.B. Bala, Acta. Crystallogr. **9,** 1019 (1956).
26. C.T. Chou, A.R. Preston, and J.W. Steeds, Philos. Mag. A**65,** 863 (1992).